

Luminescence properties of $\text{Sr}_5\text{Nb}_4\text{O}_{15}:\text{Sm}^{3+}$ reddish-orange phosphors

QIFENG TANG*, JINGQING AO, BIAO GUO, WEICAI WAN, BIYOU PENG

College of Materials Science and Engineering, Xihua University, Chengdu 610039, PR China

In this study, $\text{Sr}_5\text{Nb}_4\text{O}_{15}:\text{Sm}^{3+}$ phosphors were synthesized using a high temperature solid-state reaction method. Their phase composition, particle size distribution, morphology and photoluminescence spectra were investigated by X-ray diffraction, laser granulometry, scanning electron microscopy and fluorescence spectrometer, respectively. The XRD pattern showed that the as-prepared phosphors were single phase with no impurity, and the introduction of Sm^{3+} had little influence on the crystal structure. The particles of phosphors exhibited a good crystallization and a narrow size distribution with the average diameter of about $1\mu\text{m}$. The phosphors presented excellent near ultraviolet and blue light absorption. Under excitation at 406nm, the $\text{Sr}_5\text{Nb}_4\text{O}_{15}:\text{Sm}^{3+}$ phosphors emitted bright reddish-orange light at 601nm deriving from ${}^4\text{G}_{5/2}\rightarrow{}^6\text{H}_{7/2}$ transition of Sm^{3+} ions and the optimal doping concentration of Sm^{3+} was found to be 9mol% for emission intensity reaching to the top. The obtained results indicated that the $\text{Sr}_5\text{Nb}_4\text{O}_{15}:\text{Sm}^{3+}$ phosphors have high potential for white-light-emitting diodes application.

(Received June 11, 2020; accepted August 16, 2021)

Keywords: Solid-state reaction; Phosphor; Luminescence; Sm^{3+} ions

1. Introduction

White-light-emitting diodes (W-LEDs) are considered to be the fourth generation light source and have attracted worldwide attention because of their excellent performance, such as small size, high efficiency, fast response, long life, saving energy, protecting environment, etc. To date, the most widely-used W-LEDs are made of phosphor converted LEDs (pc-LEDs) [1-3]. One of the ways of pc-LEDs fabrication is coating red and green phosphors on blue LED chip or combining red-green-blue tri-color phosphors with near ultra violet LED chip [4, 5]. Compared with the blue and green light components, the commercial red-emitting phosphor ($\text{Y}_2\text{O}_3:\text{Eu}^{3+}$) is chemical unstable and has lower emission intensity due to releasing of sulfide gas [6-8]. Therefore, it is essential to develop desirable red phosphors with better luminescence properties and high stability.

It is known that phosphors are mainly composed of host and activator. A key factor in obtaining the excellent luminescence properties of activator ions is finding the appropriate host materials. Niobates have been extensively investigated for their potential functional applications in photorefractive, ferroelectric, piezoelectric and dielectric fields [9-13]. Recently, niobates have also been validated to serve as good candidate for the host of photoluminescence materials. There are a lot of literatures on the investigation of niobate phosphors activated with rare earth ions. Walasek et al. [14] prepared the $\text{Y}_3\text{NbO}_7:\text{Er}^{3+}$ phosphors by solid state reaction. Vishwakarma et al.

[15] synthesized the $\text{BaNb}_2\text{O}_6:\text{Eu}^{3+}$ phosphors by sol-gel method. Xiao et al. [16] used the chemical co-precipitation method to synthesize the $\text{Eu}^{3+}/\text{Dy}^{3+}$ ions doped $\text{Zn}_3\text{Nb}_2\text{O}_8$ microcrystalline phosphors. The structural and optical properties of $\text{BaNb}_2\text{O}_6:\text{Pr}^{3+}$ reddish orange emitting phosphors were studied by Jana et al. [17]. The photoluminescence properties of $\text{Ba}_2\text{NaNb}_5\text{O}_{15}:\text{Sm}^{3+}/\text{Eu}^{3+}/\text{Tb}^{3+}/\text{Dy}^{3+}$ crystals were described by Cavali et al. [18]. Xue et al. [19] discussed the energy transfer, tunable emission color and thermal stability of GdNbO_4 phosphors co-doped with Bi^{3+} , Eu^{3+} ions. However, to the best of our knowledge, few studies on the luminescence of $\text{Sr}_5\text{Nb}_4\text{O}_{15}$ doped with Sm^{3+} ions have been reported yet. Herein, in this work, we chose $\text{Sr}_5\text{Nb}_4\text{O}_{15}$ as host and Sm^{3+} ion as activator to synthesize reddish-orange emitting phosphors by a conventional high-temperature solid-state reaction method, and the phase purity, morphology and photoluminescence properties of as-prepared phosphors were investigated. The results indicated that $\text{Sr}_5\text{Nb}_4\text{O}_{15}:\text{Sm}^{3+}$ phosphors had potential in LED application.

2. Experimental

2.1. Synthesis

A series of $\text{Sr}_{5-x}\text{Nb}_4\text{O}_{15}:\text{xSm}^{3+}$ phosphors were prepared by solid state reaction. Analytical reagent grade SrCO_3 , Nb_2O_5 , and Sm_2O_3 (99.99%) were used as the initial materials, which were weighed on the basis of stoichiometric ratio and mixed homogeneously by

grinding in agate mortar for 30min. Then, the mixtures were heated at 1400°C for 6h in air. Finally, the samples were cooled down to room temperature inside the furnace and ground into powder for subsequent measurements.

2.2. Characterization

The phase composition of the as-prepared phosphors was characterized by X-ray diffraction (XRD) using a D/MAX2500 X-ray diffractometer with $\text{Cu K}\alpha$ radiation in the 2θ range from 10° to 70° . The particle size was examined by laser granulometry (JL-1177, made by JNGX Company in China). The scanning electron microscopy (SEM) system (TESCAN VAGA-3 LM), equipped with an energy dispersive X-ray (EDX) spectrometer, was used to observe the morphology of samples. The photoluminescence excitation (PLE) and emission (PL) spectra were recorded using the Hitachi F-7000 fluorescence spectrophotometer with a 150 W Xenon lamp as excitation light sources. All the measurements were carried out at room temperature.

3. Results and discussion

3.1. Phase purity and morphology

The XRD patterns of the representative samples of pure $\text{Sr}_5\text{Nb}_4\text{O}_{15}$ and $\text{Sr}_{4.91}\text{Nb}_4\text{O}_{15}:\text{0.09Sm}^{3+}$ phosphor are shown in Fig. 1. As can be seen, all the peaks of samples are matched well with the $\text{Sr}_5\text{Nb}_4\text{O}_{15}$ card of Joint Committee on Powder Diffraction standard (JCPDS, no. 48-0421) and no other impurity phases are detected, indicating that Sm^{3+} ions are effectively dissolved into the $\text{Sr}_5\text{Nb}_4\text{O}_{15}$ host lattice without causing any obvious changes of the host structure. According to the information of standard card JCPDS48-0421, $\text{Sr}_5\text{Nb}_4\text{O}_{15}$ belongs to the hexagonal $P3m1$ space group with cell parameters of $a = b = 5.6565 \text{ \AA}$, $c = 11.4586 \text{ \AA}$, $Z = 1$, and $V = 317.5 \text{ \AA}^3$. The ionic radius of cations in $\text{Sr}_5\text{Nb}_4\text{O}_{15}:\text{Sm}^{3+}$ phosphors are $R_{\text{Sr}^{2+}} = 1.26 \text{ \AA}$, $R_{\text{Nb}^{5+}} = 0.048 \text{ \AA}$ and $R_{\text{Sm}^{3+}} = 1.1 \text{ \AA}$. Taking into account the principles of similar valence states and ionic radius, Sm^{3+} should incorporate into the site of Sr^{2+} . From the XRD patterns, it also observed that the XRD peaks slightly shift to larger angles with the incorporation of Sm^{3+} ions in $\text{Sr}_5\text{Nb}_4\text{O}_{15}$ lattice. Based on Bragg's law: $2d\sin\theta = n\lambda$, where d stands for the interplanar distance

and θ represents half diffraction angle. The d would be shortened when the Sr^{2+} ions with larger ionic radius are replaced by the smaller Sm^{3+} ions, resulting that θ become bigger and thus a red shift phenomenon appears in the XRD patterns of $\text{Sr}_{4.91}\text{Nb}_4\text{O}_{15}:\text{0.09Sm}^{3+}$.

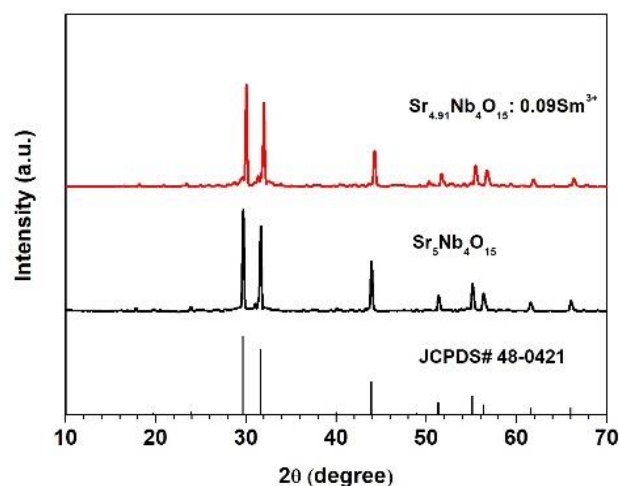


Fig. 1. XRD patterns of $\text{Sr}_5\text{Nb}_4\text{O}_{15}$, $\text{Sr}_{4.91}\text{Nb}_4\text{O}_{15}:\text{0.09Sm}^{3+}$ phosphors, and standard card (JCPDS, no. 48-0421) (color online)

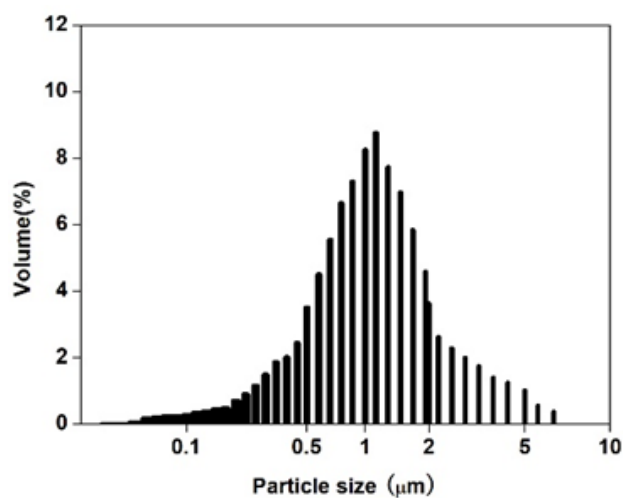


Fig. 2. Particle size distribution of $\text{Sr}_{4.91}\text{Nb}_4\text{O}_{15}:\text{0.09Sm}^{3+}$ phosphors

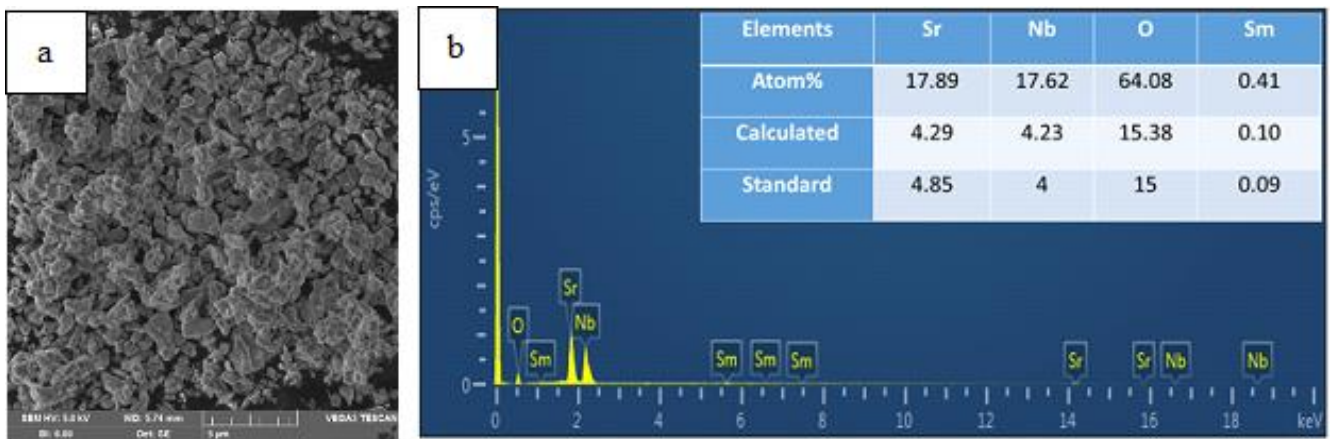


Fig. 3. SEM images (a) and SEM EDS elemental mapping (b) of Sr, Nb, O, Sm for $\text{Sr}_{4.91}\text{Nb}_4\text{O}_{15}: 0.09\text{Sm}^{3+}$ phosphors (color online)

Fig. 2 presents the particle size distribution of $\text{Sr}_{4.91}\text{Nb}_4\text{O}_{15}: 0.09\text{Sm}^{3+}$ phosphors. A narrow size distribution is obtained and the particle size varies from $0.5\mu\text{m}$ to $2\mu\text{m}$ with average size of approximately $1\mu\text{m}$. This size range is suitable for the encapsulation of w-LEDs. Meanwhile, small size is beneficial to improve the luminescent intensity of phosphors by enhancing the density of accumulations [20].

The morphology of $\text{Sr}_{4.91}\text{Nb}_4\text{O}_{15}: 0.09\text{Sm}^{3+}$ phosphors is observed from the SEM studies and shown in Fig. 3. Due to the inherent characteristics of the high temperature solid state reaction, the phosphors exhibit irregular shape and some agglomeration in Fig. 3(a). Fig. 3(b) displays the elemental composition analysis of the $\text{Sr}_{4.91}\text{Nb}_4\text{O}_{15}: 0.09\text{Sm}^{3+}$ phosphors. The EDX spectrum signifies the presence of Sr, Nb, O and Sm elements, and the Sm peaks mainly are located in 5~8 keV. The inset table in Fig. 3(b) confirms that the atom ratio of Sr: Nb: O: Sm, based on the atomic percentage, is calculated to be 4.29: 4.23: 15.38: 0.1, closing to the standard value of $\text{Sr}_{4.91}\text{Nb}_4\text{O}_{15}: 0.09\text{Sm}^{3+}$ within the allowed error. This also demonstrates that the Sm^{3+} ions doped into Sr^{2+} sites in their theoretical stoichiometry.

3.2. Luminescent properties

The excitation spectra of $\text{Sr}_{4.91}\text{Nb}_4\text{O}_{15}: 0.09\text{Sm}^{3+}$ phosphors monitored at wavelength of 600nm is shown in Fig. 4. There is a broad band in the short ultraviolet region extending from 250nm to 325nm with a maximum at about 300nm can be observed, which could be attributed to the charge transfer(CT) state of the $\text{O}^{2-}\text{-Sr}^{5+}$ and $\text{O}^{2-}\text{-Sm}^{3+}$ interaction[21]. The excitation bands in the range of 325-500nm are assigned to the intra-configurational f-f transitions of Sm^{3+} ions in the niobate. In the long ultraviolet to blue light region, the weak peaks located at 345nm, 364nm, 381nm, 418nm, 440nm and 463nm correspond to the ${}^6\text{H}_{5/2} \rightarrow {}^4\text{H}_{9/2}$, ${}^6\text{H}_{5/2} \rightarrow {}^4\text{H}_{7/2}$, ${}^6\text{H}_{5/2} \rightarrow {}^4\text{P}_{7/2}$, ${}^6\text{H}_{5/2} \rightarrow {}^4\text{P}_{5/2}$, ${}^6\text{H}_{5/2} \rightarrow {}^4\text{G}_{9/2}$ and ${}^6\text{H}_{5/2} \rightarrow {}^4\text{I}_{13/2}$ transitions, and the strong excitation peaks centered at 406nm and 484nm belong to ${}^6\text{H}_{5/2} \rightarrow {}^4\text{F}_{7/2}$ and ${}^6\text{H}_{5/2} \rightarrow {}^4\text{I}_{11/2}$ transitions,

respectively[22, 23]. The results of excitation spectra indicate that the $\text{Sr}_5\text{Nb}_4\text{O}_{15}: \text{Sm}^{3+}$ phosphors can be effectively excited by near ultraviolet and blue chips.

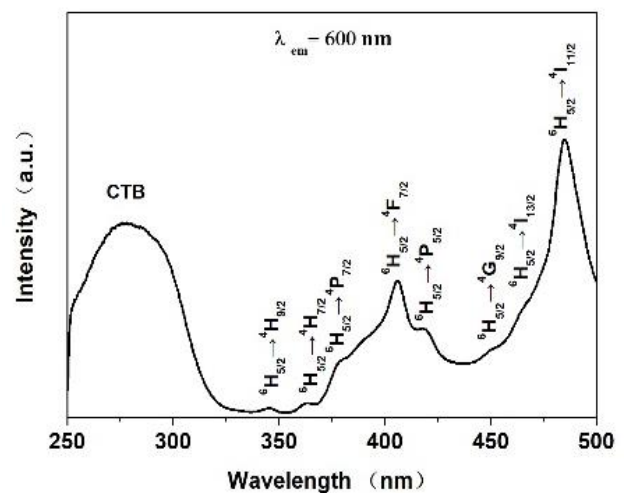


Fig. 4. PLE spectra of $\text{Sr}_{4.91}\text{Nb}_4\text{O}_{15}: 0.09\text{Sm}^{3+}$ phosphors monitored at 600nm

Fig. 5 presents the emission spectra of $\text{Sr}_{4.91}\text{Nb}_4\text{O}_{15}: 0.09\text{Sm}^{3+}$ phosphor excited at 406nm. There are three emission peaks at 562nm, 601nm and 690nm, which are related to the characteristics transitions from excited level ${}^4\text{G}_{5/2}$ to ${}^6\text{H}_{5/2}$, ${}^6\text{H}_{7/2}$ and ${}^6\text{H}_{11/2}$ of Sm^{3+} ions, respectively[22, 23]. The ${}^4\text{G}_{5/2} \rightarrow {}^6\text{H}_{7/2}$ (601nm) transition is observed to be the most intense one, indicating that the $\text{Sr}_5\text{Nb}_4\text{O}_{15}: \text{Sm}^{3+}$ phosphors can emit intense reddish-orange light under the excitation of near-ultraviolet light.

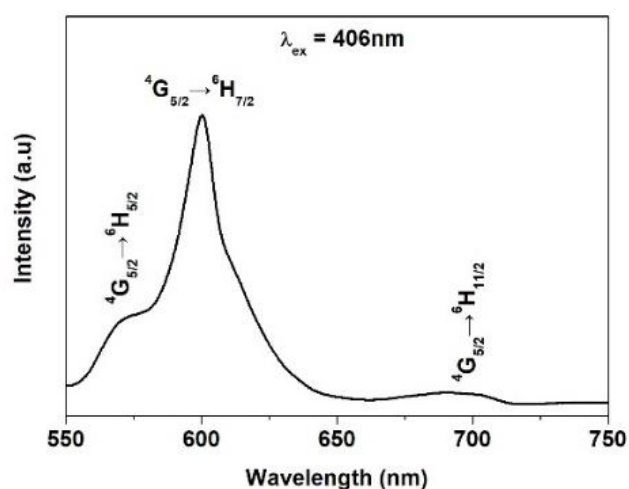


Fig. 5. PL spectra of Sr_{4.91}Nb₄O₁₅:0.09Sm³⁺ phosphors excited at 406nm

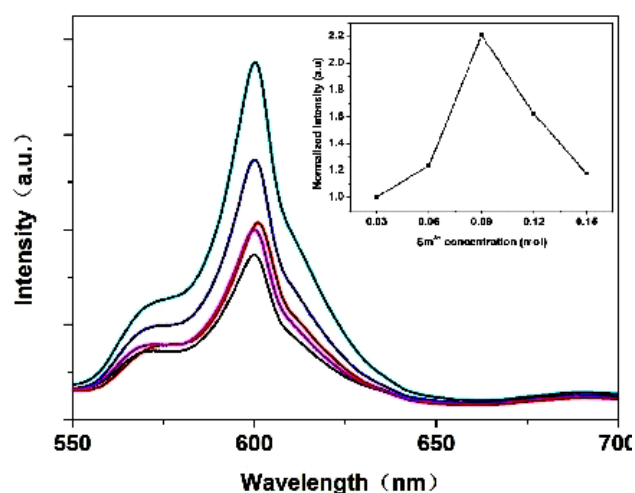


Fig.6. PL spectra of Sr_{5-x}Nb₄O₁₅:xSm³⁺ phosphors excited at 406nm with different Sm³⁺ ion concentrations (The inset shows the relationship between the emission intensity and Sm³⁺ ion concentration (color online))

The emission spectra of Sr_{5-x}Nb₄O₁₅: xSm³⁺ phosphors, where x varies from 0.03 to 0.15, are illustrated in Fig. 6. It could be clearly observed that the emission of Sr_{5-x}Nb₄O₁₅: xSm³⁺ phosphors with various doping concentrations of Sm³⁺ ions present the same dependencies in form and location except for PL intensity. Fig. 6 (inset) shows the effects of different Sm³⁺ doped concentration on the relative PL intensity. From the experimental result, the emission intensity of samples increases at first with increasing of Sm³⁺ ion concentration, consequently reaches a maximum at $x=0.09$, and then the decreases when the Sm³⁺ doped concentration exceeds 0.09. The tendency is usually caused by the concentration quenching among the Sm³⁺ ions. At lower dopant concentration, the emission intensity is mainly determined by the number of luminescence center. In this case, increase in Sm³⁺ doped concentration can provide more luminescence centers in the host, which leads to an increase in the emission intensity. However, when the doping concentration

exceeds the critical value, the cross-relaxation of luminescence centers becomes stronger, and the emission energy is dissipated by non-radiative transition due to the increasing concentration of Sm³⁺ ions. Hence, the concentration quenching behavior could occur and the emission intensity of phosphors starts to drop.

It is known that the distance between activator ions is inversely proportional to the dopant concentration, so the concentration quenching depends on the critical energy transfer distance, which is the shortest distance between nearest activator ions. The critical distance (R_c) between Sm³⁺ ions can be calculated using the following equation proposed by Blasse[24]:

$$R_c \approx 2 \left[\frac{3V}{4\pi CZ} \right]^{\frac{1}{3}} \quad (1)$$

where V stands for the volume of the unit cell, C and Z represents the critical concentration and the number of activator ions in the unit cell, respectively. According to Blasse's theory, if the critical distance (R_c) is 5 Å or less, the process of energy transfer is controlled by the exchange interaction. In this work, the analytic values of V , C and Z in the Sr₅Nb₄O₁₅: Sm³⁺ phosphors are 317.5Å³, 0.09 and 1, respectively. By calculation, the critical distance (R_c) is approximately 19Å, which is larger than 5Å. Thus, we can conclude that the energy transfer mechanism in Sr₅Nb₄O₁₅: Sm³⁺ phosphors is not dominated by the exchange interaction, but by multipolar interaction.

There are three types of energy transfer for multipolar interaction, namely, the electric dipole-dipole(d-d), electric dipole-quadrupole(d-q) and electric quadrupole-quadrupole (q-q) interaction. Based on Van Urtter's energy transfer model of multipolar interaction, the exact interaction type between activators can be determined by the relationship between the emission intensity and activate ions concentration, as expressed below[26]:

$$I = \frac{x}{k[1 + \beta(x)^{\theta/3}]} \quad (2)$$

where x is Sm³⁺ doped concentration, not less than the critical concentration, k and β are constants for the same excitation condition for a given host lattice, θ is electric multipolar character. The values of θ in this formula are 6, 8 and 10 correspond to the d-d, d-q and q-q interactions, respectively. The dependence of $\log(I/x)$ on $\log(x)$ is depicted in Fig. 7. The slope ($\theta/3$) of linear fitting function is -2.23 and the value of θ is calculated to be 6.69, which is close to 6. This indicating that the energy transfer between Sm³⁺ ions is due to the electric dipole-dipole interaction in Sr₅Nb₄O₁₅: Sm³⁺ phosphors.

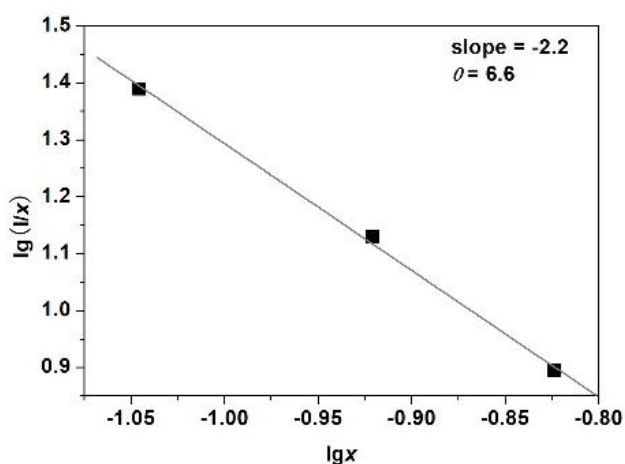


Fig. 7. Relationship between $\log(I/x)$ and $\log(x)$ in $Sr_{5-x}Nb_4O_{15}:xSm^{3+}$ phosphors ($\lambda_{ex} = 406nm$)

4. Conclusions

A series of new $Sr_5Nb_4O_{15}:Sm^{3+}$ reddish-orange emitting phosphors were successfully prepared by conventional high-temperature solid-state reaction method at $1400^\circ C$ for 6h in air. The XRD pattern demonstrates that phase pure phosphors was obtained and the introduction of Sm^{3+} did not change the host crystal structure. The substitution of Sm^{3+} for Sr^{2+} in $Sr_5Nb_4O_{15}$ phosphor results a red shift phenomenon in the XRD pattern. The particle size of phosphors varies from $0.5\mu m$ to $2\mu m$ with average size of about $1\mu m$, indicating that the particle is suitable for fabricating of w-LEDs. The photoluminescence measurements show that the $Sr_5Nb_4O_{15}:Sm^{3+}$ phosphors could be effectively excited by near ultraviolet and blue light, and emit bright reddish-orange light. Upon excitation at $406nm$, the phosphors exhibit intensity reddish-orange emission at $601nm$ corresponding to the ${}^4G_{5/2} \rightarrow {}^6H_{7/2}$ transition of Sm^{3+} . In addition, the photoluminescence intensity is dependent on the concentration of Sm^{3+} , and the strongest emission intensity was achieved in $Sr_{4.91}Nb_4O_{15}:0.09Sm^{3+}$ phosphor. The critical distance (R_c) was approximately 19\AA by calculation, the energy transfer mechanism in $Sr_5Nb_4O_{15}:Sm^{3+}$ phosphors is dominated by multipolar interaction. The $Sr_5Nb_4O_{15}:Sm^{3+}$ phosphor may be a promising phosphor candidate for applications in white-light-emitting diodes.

Acknowledgements

This work was financially supported by the General Project of Sichuan Province Department of Science and Technology Fund for Nature (Grant No. 2019YFG70511) and Key Scientific Research Fund of Xihua University (Grant No. z1320109).

References

- [1] Y. H. Wang, Y. Gong, X. H. Xu, Y. Q. Li, J. Lumin. **133**, 25 (2013).
- [2] H. Q. Jia, L. W. Guo, W. X. Wang, H. Chen, Adv. Mater. **21**(45), 4641 (2009).
- [3] A. P. Shablinskii, I. E. Kolesnikov, R. S. Bubnov, J. Lumin. **216**, 1 (2019).
- [4] C. Y. Shen, Y. Yang, S. Z. Jin, Phys. B **404**(8-11), 1481 (2009).
- [5] P. C. Chen, L. Z. Zhou, F. W. Mo, Mater. Res. Bull. **72**, 191 (2015).
- [6] S. Ye, F. Xiao, Y. Pan, Y. Ma, Q. Zhang, Mater. Sci. Eng. R. **71**(1), 1 (2010).
- [7] C. C. Lin, R. S. Liu, J. Phys. Chem. Lett. **2**(11), 1268 (2011).
- [8] L. D. Carlos, R. S. Ferreira, V. Z. Bermudez, B. Julian-Lopez, P. Escribano, Chem. Soc. Rev. **40**(2), 536 (2012).
- [9] J. Leitner, M. Hampl, K. Ruzicka, Thermochim. Acta **475**(1-2), 33 (2008).
- [10] J. K. Chang, G.H. Soon, Thin Solid Films **365**(1), 58 (2000).
- [11] P. P. Rao, S. J. Liji, K. R. Nair, P. Koshy, Mater. Lett. **58**(12-13), 1924 (2004).
- [12] Y. X. Li, G. Chen, H. J. Zhang, Z. H. Li, Mater. Res. Bull. **44**(4), 741 (2009).
- [13] H. P. Ning, H. X. Yan, M. J. Reece, J. Am. Ceram. Soc. **93**(5), 1409 (2010).
- [14] A. Walasek, E. Zych, J. Zhang, S.W. Wang, J. Lumin. **127**(2), 523 (2007).
- [15] A. K. Vishwakarma, M. Jayasimhadri, J. Alloys. Compd. **683**, 379 (2016).
- [16] X. Z. Xiao, B. Yan, Mater. Sci. Eng. B **136**(2-3), 154 (2007).
- [17] S. Jana, A. Mondal, J. Manam, S. Das, J. Alloys. Compd. **821**, 1 (2020).
- [18] E. Cavalli, A. Belletti, R. Mahiou, J. Lumin. **130**(4), 733 (2010).
- [19] J. P. Xue, H. M. Noh, B. M. Choi, Chem. Eng. J. **382**, 1 (2020).
- [20] Z. J. Liang, F. W. Mo, X. G. Zhang, L. Y. Zhou, Ceram. Intl. **40**(5), 7501 (2014).
- [21] F. H. Xue, Y. H. Hu, X. H. Lin, L. M. Fan, Displays **52**, 40 (2018).
- [22] P. Kumari, Y. Dwivedi, Optik. **203**, 1 (2020).
- [23] H. F. Guo, Q. F. Shi, V.I. Konstantin, Mater. Res. Bull. **126**, 1 (2020).
- [24] Q. Yang, G. F. Li, Y. G. Wei, H. Y. Chai. J. Lumin. **199**, 323 (2018).
- [25] G. Blasse. Phys. Lett. A **28**(6), 444 (1968).
- [26] D. L. Dexter, J. H. Schulamn, J. Chem. Phys. **15**(22), 1063 (1954).

*Corresponding author: tqfkmust@126.com